

Measurement of electron temperatures of Argon Plasmas in a High-Density Inductively-Coupled Remote Plasma System by Langmuir Probe and Optical-Emission Spectroscopy

A. Boogaard, A. Y. Kovalgin, A. A. I. Aarnink, R. A. M. Wolters, J. Holleman,
I. Brunets, J. Schmitz

Abstract— We measured electron density and electron energy distribution function (EEDF) in our reactor by a Langmuir probe. The EEDF of Ar plasma in the reactor could largely be described by the Maxwell-Boltzmann distribution function, but it also contained a fraction ($\sim 10^{-3}$) of electrons which were much faster (20-40 eV). The peak of the fast-electron tail shifted from $E \sim 35$ eV at 11 μ bar to $E \sim 25$ eV when we increased pressure to 120 μ bar or applied an external magnetic field of 9.5 μ T. We also measured *relative* mean electron temperatures (kT_e) by optical emission spectroscopy (OES). This method is especially sensitive to the fraction of fast electron in the plasma. The relative kT_e measured by OES decreased from 1.6 eV at 11 μ bar to 1.4 eV at 120 μ bar. OES can be used, in addition to Langmuir-probe measurements, when depositing plasmas are used. Combining the Langmuir-probe and OES measurements in non-depositing plasmas, we can further verify the EEDF in depositing plasmas by means of OES measurements only. Knowing EEDF in e.g. silane-containing plasmas is very important for chemical modeling.

Index Terms— PECVD; ICPECVD; Langmuir probe; OES; EEDF, electron temperature

I. INTRODUCTION

WE built an Inductively-Coupled Remote Plasma-Enhanced Chemical Vapor Deposition (ICPECVD) system for deposition of dielectric and semi-conducting layers at low substrate temperatures (~ 150 °C). The deposition system was designed to operate either in a chemical-vapor-deposition (CVD) or atomic-layer-deposition (ALD) mode. Both are promising techniques to deposit layers with good electrical properties at low substrate temperatures. This apparatus will be used to study the influence of physics and chemistry on the deposition process and on the electrical and

physical properties of the deposited films. To do so, we need to characterize the plasma by identifying and measuring plasma species and by relating plasma characteristics to film properties.

We performed Langmuir-probe measurements in order to obtain data for the chemical modeling of our deposition processes. To model electron-stimulated reactions in plasma, one should know the reaction cross-sections, partial pressures of reactants, electron densities and electron energy distribution functions (EEDF) [1]. Langmuir-probe measurements can provide us the EEDF and electron densities. These measurements allow for modeling of chemical processes in plasmas, and will thus result in a better understanding and optimization of the deposition process. However, it is not possible to perform Langmuir-probe measurements when silane is present in the chamber, because it will form deposits on the probe. To overcome this problem, mean electron temperature [2] can be determined by means of Optical Emission Spectroscopy (OES) in depositing plasmas. In addition to Langmuir probe measurements, OES can provide concentrations of certain particles (e.g., Si and SiH radicals) [3].

In this work, we compare electron temperatures extracted from both Langmuir-probe and OES measurements, carried out for argon plasmas at various process conditions.

II. EXPERIMENTAL

A. Deposition System

Figure 1 schematically shows the system set-up. The inductive-coupled plasma source (supplied by Alcatel Micro Machining Systems; 13.56 MHz, max. electric power of 2 kW) is placed on top of the chamber (also supplied by Alcatel). Quoted electric powers are measured at the output of the rf generator (RF power products, model FR20S), and are not corrected for losses in the matching network.

The ICP-source is also equipped with external DC coils (item (3) in Fig. 1) which can induce an axial magnetic field to improve the ionization and power absorption efficiency of the plasma. The maximum magnetic field that can be applied (by

This work was supported by the Dutch Technology Foundation (STW), under project STW-TEL 6358.

All Authors are with the MESA+ Research Institute, Chair of Semiconductor Components, University of Twente, P.O. Box 217, 7500 AE Enschede, The Netherlands. (Corresponding author is A. Boogaard; phone: +31 53 489 2727; fax: +31 53 489 1034; e-mail: a.boogaard@utwente.nl)

setting the current through the coil) is 9.5 μ T.

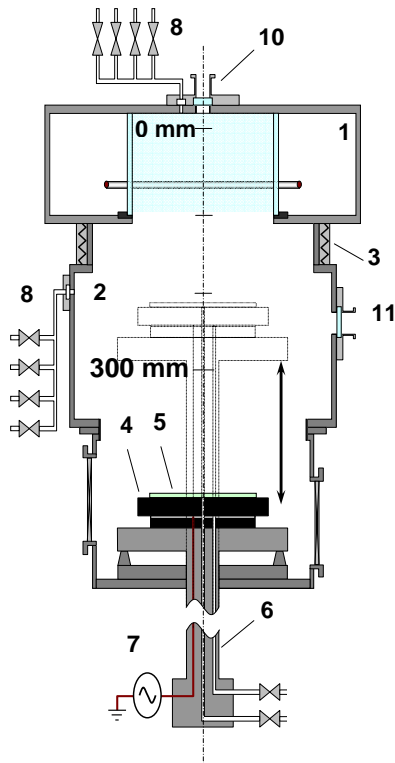


Fig. 1. A schematic drawing of the remote-plasma CVD system: (1) ICP source, (2) chamber, (3) DC coil to introduce axial magnetic field, (4) chuck and susceptor, (5) wafer, (6) motor-driven arm, (7) rf-source for chuck biasing, (8) gas-inlets, (9) gas-inlet to control pressure between wafer and susceptor, and between susceptor and chuck, (10) port to introduce Langmuir probe, (11) glass window; the gas distribution system, load lock and vacuum pumps are not shown.

The wafer is placed in the load lock on a molybdenum susceptor. After a pump-down cycle, the wafer is transferred into the chamber by an automated arm, and positioned on the chuck. The chuck is situated at the bottom of this chamber. The chuck can be heated up to 400 °C, but the targeted deposition temperatures should not exceed 150 °C. Temperature is controlled by a PID (proportional-integral-derivative) controller via a thermo-couple inserted into the chuck. The wafer is mechanically clamped to the chuck. Argon backing pressure of 10 mbar between the susceptor and the chuck and between the wafer and the susceptor guarantees a fairly good heat transfer between the chuck and the wafer [4]. The chuck can be rf-biased and can be moved upwards into the chamber, i.e., towards the plasma source. Furthermore, in Figure 1 two gas inlets are shown: one above the plasma source and one below, in the chamber. An extensive gas distribution system (not shown in the figure) will supply gases to the deposition system, eventually in a pulsed mode. Mass flow controllers (Bronkhorst High-Tech B.V.) are used to control the gas flows. The system is evacuated with an oil-free turbo molecular pump (Adixen ATH 1300 M, effective argon pumping speed 800 l/min) backed by a dry pump (Adixen ACP 40 G); base pressure is

5·10⁻⁷ mbar. A set of Pfeiffer capacitance gauges is used for accurate measurement of process pressures (Pfeiffer CMR 261 and CMR 263), whereas a combined cold wall and Pirani gauge (Pfeiffer PKR 261)) measures from base pressure to atmospheric pressure.

Via the load lock, our system is connected to two thermal ALD-systems (aimed at deposition of metal barriers and dielectrics), and to an XPS and AFM/STM measurement tool. In future, these measurement tools will be used to study both the film composition and morphology without vacuum break.

B. Plasma operation conditions

In all the experiments described in this work, argon was used as a carrier gas. The process pressure ranged from 6.8 to 120 μ bar, while the argon flow varied between 300 and 500 sccm. Process pressure was controlled by a feedback loop to the throttle valve.

C. Langmuir probe

An rf-compensated Langmuir probe (Scientific Systems SmartProbe™) was used for plasma diagnostics. The active part of the Langmuir probe is a tungsten wire of 0.19 mm in diameter and 10 mm in length. The probe tip is connected to an acquisition unit via a coaxial cable that is shielded from the plasma by an alumina shaft. The shaft length is 470 mm and its diameter is 9.5 mm. The shaft is mounted onto a linear drive system so that the probe can be moved in vertical direction. The drive system is placed on top of the ICP source (see Fig. 1). This system consists of vacuum bellows, a stepping motor and a precision ball screw arrangement. Typically, probe current is measured at bias voltages in the range from -60 to +60 V. The drive system enables measuring the plasma parameters vertically through the plasma-generation zone downwards to the chuck (i.e., at locations between 0 and 300 mm on the axis shown in Figure 1). However, the horizontal optical axis, used for monitoring the OES spectra, crosses the vertical axis at 240 mm. Therefore, the presented OES data are compared with the Langmuir-probe data measured at this position.

The problems associated with Langmuir probes in rf plasmas are well known and described in [5], [6]. *Hirsch* concluded that for non-compensated probes, the apparent distribution of electrons (as measured by the probe) is a function of rf interactions in the probe sheath, rather than a function of electron energy distribution in plasma. Additionally, *Paranjpe et al.* showed that the rf voltage across the probe-plasma sheath caused a time dependent variation of the plasma potential, which very much affected the measured electron energy distribution.

The most common solution to minimize this rf distortion is provided by the manufacturers of such probes [7] and it involves increasing the probe-to-ground impedance. This ensures that the rf voltage drop mainly occurs between the probe and the ground and not between the plasma and the sheath.

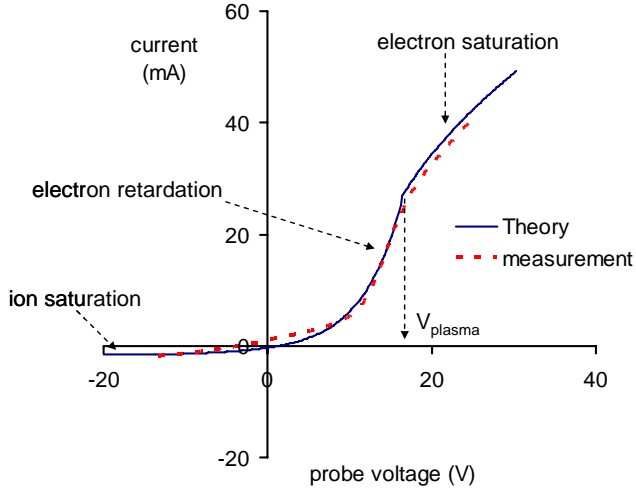


Fig. 2. Typical Langmuir-probe measurement in our deposition system. (---) Measurement in Ar plasma at 11 μ bar and 300 W ICP power, probe at 240 mm; (—) Laframboise theory fitted to those data.

A current will be collected from plasma when the probe tip is DC biased with respect to plasma, which results in an I - V curve, as depicted in Figure 2. Figure 2 also shows the curve as derived from Laframboise theory [8]. One can see good agreement between the measured and theoretical curves. The plasma potential (V_p) is defined as the voltage at the transition point between the electron retarding and the electron saturation parts of the curve, i.e., where the second derivative is zero ($V_p = 16.6$ V in Figure 2). The mean electron temperature (kT_e) can be determined from the slope of the $\ln(I)$ - V curve in the region on the left-hand side from V_p . Next, electron density (n_e) can be calculated from the current measured at V_p using the following equation:

$$n_e = \frac{I(V_p)}{A_{probe}} \sqrt{\frac{2\pi m_e}{e^2 kT_e}} \quad (1)$$

where A_{probe} is the surface area of the probe, m_e is the free electron mass, e is the electron charge and kT_e is the mean electron temperature in eV.

The Druyvesteyn [9] extension of the Langmuir and Mott-Smith theory [10] allows the determination of the EEDF. *Druyvesteyn* showed that the EEDF could be found from the expression,

$$N(\varepsilon) = n_e f(E) = \frac{2}{e^2 A_{probe}} \sqrt{\frac{2m_e \varepsilon}{e}} \frac{d^2 I}{dV^2} \quad (2)$$

where $N(\varepsilon)$ is the number of electrons within energy domain $e(\varepsilon + d\varepsilon)$ eV, V is the probe voltage, ε is the probe potential with respect to the plasma potential V_p , ($\varepsilon = V_p - V$), A_{probe} is the probe surface area, $d^2 I/dV^2$ is the second derivative of the electron current with respect to the electron energy ε , and e and m_e are the electron charge and free mass.

In this paper, the second derivative of the I - V curve is

calculated numerically and averaged over 1000 values at each point on the I - V curve, to reduce noise. The electron density, n_e , can also be obtained from the following integral,

$$n_e = \int_0^\infty N(\varepsilon) d\varepsilon \quad (3)$$

In theory, the n_e thus obtained should equal the measured n_e at V_p (see Eq. 1). In practice, these two values can differ by a factor of two.

D. Optical Emission Spectroscopy

Spectra were acquired using an optical fiber, by collecting photons emitted from the glass window mounted on the chamber wall. The horizontal optical axis crossed the vertical axis in Fig. 1 at a vertical position of 240 mm. The fiber output was connected to an Avantes AVS-SD2000 spectrophotometer with an optical resolution of 0.5 nm. The measured spectral range was 250-1100 nm, although only the emission lines between 600 and 700 nm were used to extract mean electron temperature. Fig. 3 shows a typical Ar plasma emission spectrum.

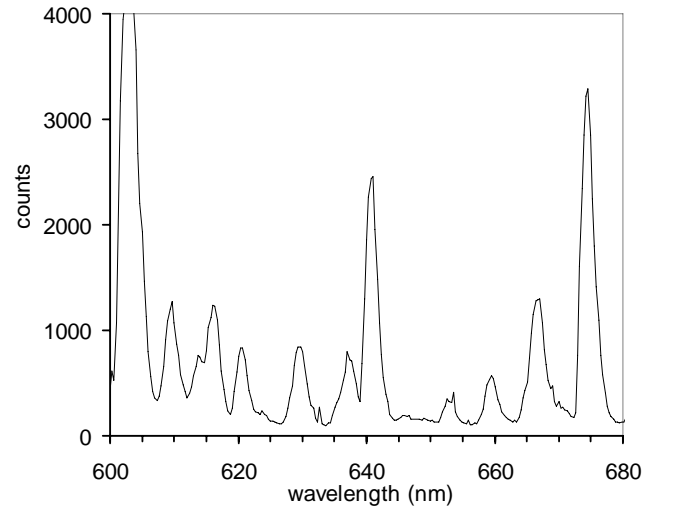


Fig. 3. Typical Ar plasma emission spectrum, recorded at a position of 240 mm on the axis shown in Fig. 1; $p = 11 \mu$ bar, ICP power 300 W, Ar flow 500 sccm; spectrometer integration time 3 s.

Collisions between unexcited argon atoms and sufficiently-energetic electrons are the dominant mechanism leading to their excitation in low-temperature plasmas. The radiation in the range from UV to NIR, originating from the excited species, consists of a number of emission lines corresponding to the (known) transitions between discrete electronic levels of these species. According to [2], the intensity of such a radiation can be expressed by

$$I_1 \propto h\nu_1 A_1 n_1 \propto h\nu_1 A_1 n_{Ar} n_e \sigma(E) \quad (4)$$

where I_1 is the radiation intensity of transition 1, h is Planck's constant, ν_1 is the frequency of transition 1, A_1 is the transition probability from the excited state to a lower state, n_1 is the density of argon atoms excited to state 1, n_{Ar} and n_e are the argon and electron densities, and $\sigma(E)$ is the excitation cross

section. Assuming Maxwell-Boltzmann energy distribution for the electrons in plasma, the mean electron temperature kT_e can be extracted (see ref. [2] for details) from equation (5), by measuring the relative intensities of two emission lines I_1 and I_2 :

$$\ln\left(\frac{I_1}{I_2} \frac{C_2 v_2 A_2 (E_2 + 2kT_e)}{C_1 v_1 A_1 (E_1 + 2kT_e)}\right) = (E_2 - E_1) / kT_e, \quad (5)$$

where I_1 and I_2 are the intensities of emission lines assigned to transitions 1 and 2, C_1 and C_2 are proportionality constants relating the corresponding excitation cross sections $\sigma_1(E)$ and $\sigma_2(E)$ to electron energy, E_1 and E_2 are the threshold energies for transitions 1 and 2, and kT_e is the mean electron temperature. The kT_e values from the emission spectra were calculated assuming the ratio C_2/C_1 to be 1 [11]. In this light, the described method gives a relative value of kT_e . Table I summarizes the important characteristics of several electronic transitions of Ar, used in this study. The emission lines were chosen 1) to eliminate overlapping with the lines from other plasma species, and 2) to be in the same wavelength range (due to sensitivity- and adsorption-related issues).

TABLE I
ARGON ELECTRONIC TRANSITION CHARACTERISTICS [FROM REF. 12]

Species	Transition	Arbitrary transition line number	λ (nm)	A (s^{-1})	Excitation Energy (eV)
Ar ⁺	3d-4p	1	617.2	2.00E+07	21.127
Ar	4p-6s	2	641.6	1.16E+06	14.839
Ar	4p-6s	3	638.5	4.21E+05	14.848
Ar	4p-4d	4	675.3	1.93E+06	14.743

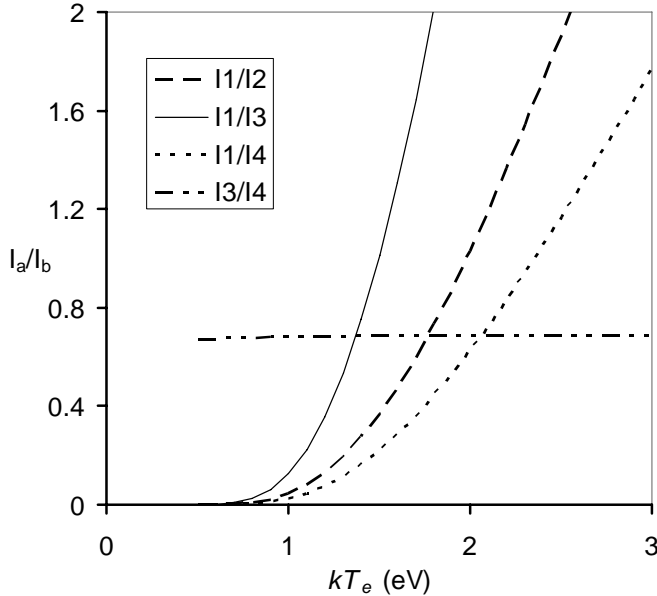


Fig. 4. Intensity ratios of several emission lines plotted as a function of kT_e , calculated from Eq. (5). Intensities I_1 - I_4 correspond to transition lines 1-4 in Table I, respectively.

Making use of Eq. 5, we plotted intensity ratios between the emission lines shown in Table I, as a function of kT_e . Comparing the curves in Fig. 4, one can draw two conclusions regarding sensitivity of this method. First, the sensitivity strongly depends on the difference in excitation energies between the two transition lines. For example, the ratio between I_1 and I_3 ($(E_1-E_3)=6.279$ eV) is a much stronger function of kT_e than the ratio between I_3 and I_4 ($(E_3-E_4)=0.105$ eV). Second, the sensitivity is affected by the ratio of the transition probabilities. For example, I_1/I_3 ($A_1/A_3=47.5$) is a stronger function of kT_e than I_1/I_2 ($A_1/A_2=17.2$) although the differences in their excitation energies are nearly the same. Therefore, to achieve good sensitivity in our study, we will calculate kT_e from the ratios I_1/I_2 , I_1/I_3 and I_1/I_4 . In other words, we will compare the emission intensity of ionized argon Ar⁺ with excited argon Ar^{*}, i.e., I_{Ar^+}/I_{Ar^*} .

III. RESULTS AND DISCUSSION

Figure 5 shows the electron energy distribution at several pressures (11, 36 and 120 μ bar) at a probe position of 240 mm (e.g., the point where the Langmuir-probe axis and the OES-measurement axis cross each other). It is important to bear in mind that zero energy means that the probe is at plasma potential. Energy of 50 eV therefore corresponds to a negative probe potential of -50 V with respect to plasma potential. The vertical axis depicts the number of electrons within the energy domain $e(\varepsilon + d\varepsilon)$. The straight lines correspond to the Maxwell-Boltzmann approximation of the energy distribution for a system in thermal equilibrium. One can see that the largest fraction of the electrons in our plasma is indeed in thermal equilibrium. However, we also measure a fraction of electrons ($\sim 10^{-3}$), which are much faster. These fast electrons can significantly influence the plasma composition, which makes them important for the chemical modeling. This is illustrated in Table II. The Table shows threshold energies for several electron-stimulated reactions in argon plasma, and the fraction of electrons with energies higher than these thresholds for both the Maxwell-Boltzmann and experimentally measured energy distribution at 11 μ bar. At high energies, the measured amount of electrons capable of exciting argon atoms seems to be 2.5 times higher than that calculated from Maxwell-Boltzmann distribution. For the ionization, the difference between the Maxwell-Boltzmann distribution and experiment becomes one order of magnitude higher.

Comparing the energy distributions of the slow (i.e., Maxwell-Boltzmann) electrons at different pressures (Fig. 5), one can see that the mean electron energy decreases with increasing the pressure. This can be explained by a shorter mean free path at higher pressures, reducing the acceleration time between two collisions. Furthermore, the peak corresponding to fast electrons shifts to lower energies at higher pressures. This could also be caused by the decreased mean free path by which the fast electrons can pick up less energy from the electric field.

TABLE II

SEVERAL ELECTRON-STIMULATED REACTIONS IN AR-PLASMA AND THEIR APPEARANCE POTENTIALS (E_0) [13]. FRACTIONS OF ELECTRONS WITH ENERGIES HIGHER THAN E_0 ARE SHOWN. WHEN CALCULATING THE FRACTIONS, THE EXPERIMENTAL EEDF AT 11 μ BAR AND THE MAXWELL-BOLTZMANN DISTRIBUTION [14] ARE COMPARED. SEE FIG. 5 FOR DETAILS.

Reaction	E_0 (eV)	$f(\epsilon > E_0)$	
		Practical	M-B
$e^- + \text{Ar} \rightarrow \text{Ar}^* + e^-$	11.56	8.6E-03	3.2E-03
$e^- + \text{Ar} \rightarrow \text{Ar}^+ + 2e^-$	15.76	7.1E-03	3.5E-04

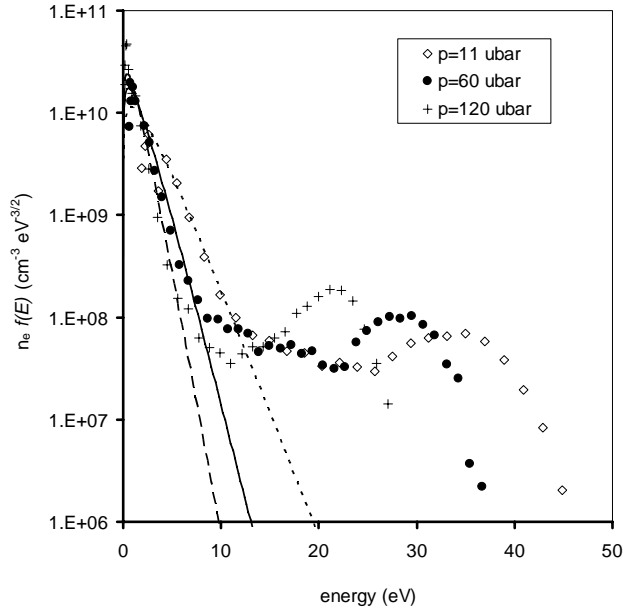


Fig. 5. EEDFs for Ar plasmas at several pressures. Probe positions: 240 mm; ICP power: 300 W. The symbols represent the measurements and the (dotted) lines represent the Maxwell-Boltzmann distribution fitted to those measurements. Mean electron energies used for the Maxwell-Boltzmann distributions are: $kT_e = 1.7$ eV at 11 μ bar, $kT_e = 1.2$ eV at 36 μ bar and $kT_e = 0.9$ eV at 120 μ bar.

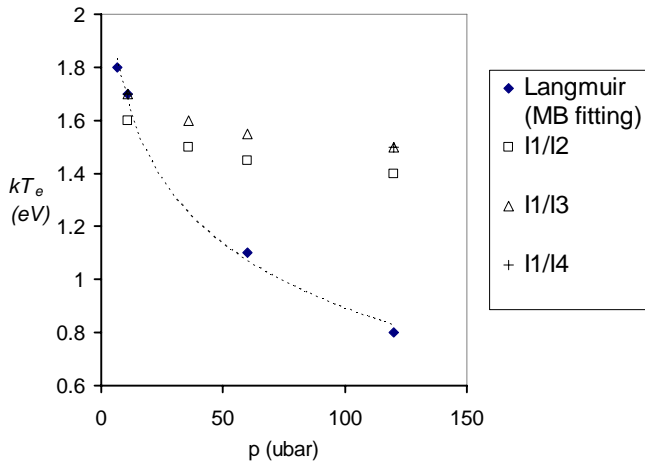


Fig. 6. Mean electron temperature measured by OES and Langmuir-probe at several pressures. All measurements are done at a position of 240 mm, ICP power of 300 W, and Ar flow rate of 500 sccm.

We also measured the line intensities of transitions from 1 to 4 (see Table I) at several pressures and calculated the corresponding mean electron temperatures. The results are presented in Fig. 6 in comparison with the mean electron temperatures extracted from the Langmuir probe measurements. The latter corresponds to the straight lines in Fig. 5).

In fig. 6, one can see good agreement between the OES and Langmuir-probe measurement results at a low pressure of 11 μ bar. However, mean electron temperatures calculated from Langmuir-probe measurements decrease much faster with increasing the pressure than those of OES measurements. This discrepancy can be explained as follows. First, the Maxwell-Boltzmann fit of the Langmuir-probe data does not take into account the fast-electron tail (see Fig. 5). On the other hand, the OES-based calculations assume Maxwell-Boltzmann distribution to be valid in the energy range from 14.7 and 21.1 eV, which covers the Ar^+ and Ar^* emission. This energy range, according to Fig. 5, lies however not in the Maxwell-Boltzmann part of the EEDF but in the fast-electron tail. The fraction of Ar^+ and Ar^* in the plasma is not significantly effected by the slow electrons and, consequently, a sharp decrease in the kT_e , as measured by the Langmuir probe (see Fig. 6), is not observed by OES. Instead, a more gradual decrease of kT_e is measured, which can be attributed to the shift of the fast-electron tail to lower energies at higher pressures (see Fig. 5). This shift should influence both the Ar^+ and Ar^* densities in plasma. However, it appears from the OES measurements that their density ratio and hence their light emission ratio are only slightly changed.

We can conclude from these observations that kT_e , as measured by OES, is hardly sensitive to the energy distribution of slow electrons. Instead, these measurements reflect the distribution of the fast electrons.

The ionization degree in plasma can be increased by applying an external axial magnetic field. Due to the Lorentz force, the length of the electron trajectory is increased, which results in more frequent collisions and better ionization efficiency [15]. The measurements show that the electron density increases from $n_e = 1.4 \cdot 10^{10}$ cm^{-3} (no magnetic field) to $n_e = 3.0 \cdot 10^{10}$ cm^{-3} (external magnetic field of 9.5 μ T calculated at a distance of 240 mm).

The EEDF is also affected by the external magnetic field; as shown in Fig. 7.

In Fig. 8, one can further see that the mean electron temperature for the slow electrons (i.e., Maxwell-Boltzmann part) slightly decreases with increasing the field strength. The shift of the fast-electron tail to lower energies (Fig. 7) is at the same time much more pronounced. These two effects can be explained as follows. Electron trajectories are deviated by a Lorentz force, which is proportional to the product of magnetic field intensity and electron velocity. So, fast electrons are deviated more effectively than slow electrons. This will result in a higher number of collisions for fast electrons. Fig. 8 compares the mean electron temperatures for

several magnetic fields, as measured by Langmuir-probe and OES. One can see a weak influence of the field on the electron temperatures measured by OES. To explain the difference between the Langmuir-probe and OES measurements, it has to be emphasized again that the fraction of Ar^+ and Ar^* in our plasma is only slightly effected by the shift of the fast-electron tail to lower energies. Consequently, a sharp decrease in the kT_e , as measured by the Langmuir probe, is not observed by OES.

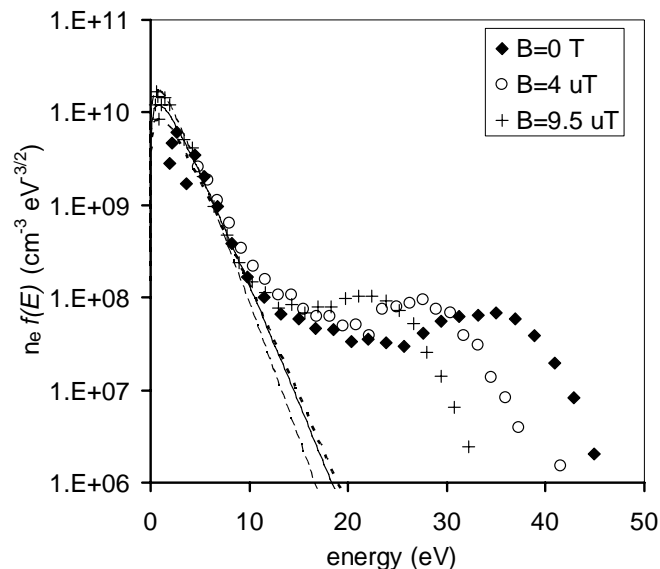


Fig. 7. EEDFs for Ar plasmas (11 μbar , 300 W ICP power) measured for various magnetic field intensities at a probe position of 240 mm. The symbols correspond to the measurements and the straight lines represent the Maxwell-Boltzmann distribution fitted to those measurements.

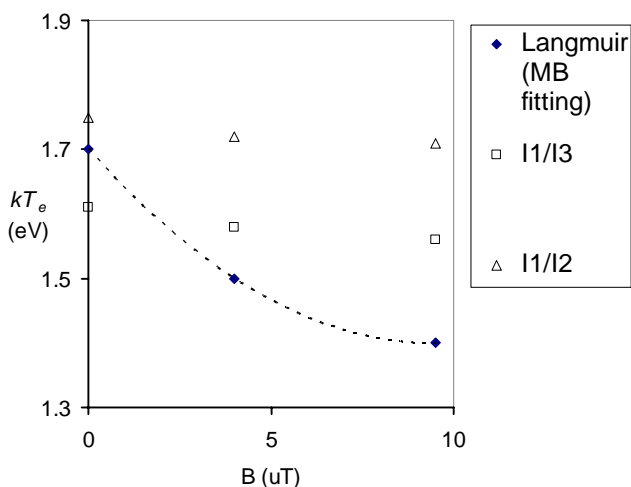


Fig. 8. Mean electron temperature measured by both OES and Langmuir-probe at various magnetic fields. All data is measured at a position of 240 mm, ICP power of 300 W, pressures of 11 μbar , and Ar flow rate of 500 sccm.

IV. CONCLUSIONS

We presented our results on a series of Langmuir-probe and OES measurements, which were carried out for

characterization of a High-Density Inductively-Coupled Remote Plasma-Enhanced Chemical Vapor Deposition (remote ICPECVD) system. We measured electron densities, electron energy distribution functions and mean electron temperatures in Ar plasmas. We compared the capabilities of Langmuir-probe and OES techniques in order to measure mean electron temperatures in such plasma systems.

The measured EEDFs exhibited two different components: a large part of slow electrons, following Maxwell-Boltzmann energy distributions, and a smaller part ($\sim 10^{-3}$) of fast electrons in the energy range of 20 to 40 eV, deviating from Maxwell-Boltzmann distribution.

The mean electron temperatures measured by OES reflected the energies of the fast electrons in plasma. This was an important observation since the fast electrons were considered to be important for the occurrence of chemical reactions in plasma. The OES measurements should be very useful for our future work, to verify the electron energy distribution in depositing plasmas, when, e.g., silane is added as a precursor.

ACKNOWLEDGMENT

The authors would like to thank Alcatel for supplying the ICP source, deposition chamber and Langmuir probe. The ICP system was designed and realized in close cooperation with 'Techno Centre for Education and Research' of the University of Twente.

REFERENCES

- [1] Haller, I., "Importance of chain reactions in the plasma deposition of hydrogenated amorphous silicon," *Journal of Vacuum Science & Technology A: Vacuum, Surfaces, and Films*, vol. 1, no. 3, pp. 1376-1382, July 1983.
- [2] Suzuki, H. and Nobata, K., "Measurements of hydrogen atom density in a Z-discharge plasma using intensities of H/sub alpha / and H/sub beta / lines," *Japanese Journal of Applied Physics, Part 1 (Regular Papers & Short Notes)*, vol. 25, no. 10, pp. 1589-1593, Oct. 1986.
- [3] Kessels, W. M. M., van de Sanden, M. C. M., and Schram, D. C., "Film growth precursors in a remote SiH4 plasma used for high-rate deposition of hydrogenated amorphous silicon," *Journal of Vacuum Science & Technology A*, vol. 18, no. 5, pp. 2153-2163, 2000.
- [4] van Graven, A. M. and Wolters, R. A. M., "Wafer temperature measurement in PVD systems using the Co-Si reaction," *Microelectronic Engineering*, vol. 50, no. 1-4, pp. 495-499, Jan. 2000.
- [5] Hirsch, E. H., "Plasma Probes and Langmuir Paradox," *International Journal of Electronics*, vol. 19 pp. 537-548, 1965.
- [6] Paranjpe, A. P., McVittie, J. P., and Self, S. A., "A tuned Langmuir probe for measurements in rf glow discharges," *Journal of Applied Physics*, vol. 67, no. 11, pp. 6718-6727, June 1990.
- [7] Gagne, R. R. J. and Cantin, A., "Investigation of an rf Plasma with Symmetrical and Asymmetrical Electrostatic Probes," *Journal of Applied Physics*, vol. 43, no. 6, pp. 2639-2647, June 1972.
- [8] Clements, R. M., "Plasma diagnostics with electric probes," *Journal of Vacuum Science and Technology*, vol. 15, no. 2, pp. 193-198, Mar. 1978. M. Young, *The Technical Writers Handbook*. Mill Valley, CA: University Science, 1989.
- [9] Druyvesteyn, M. J., "Der Niedervoltbogen," *Zeitschrift für Physik A Hadrons and Nuclei*, vol. 64, no. 11 - 12, pp. 781-798, Sept. 1930.
- [10] Langmuir, I. and Mott-Smith, H., "Studies of Electric Discharges in Gases at Low Pressures," *General Electric Review*, vol. 27, no. 7, pp. 449-455, July 1924.

- [11] Felts, J. and Lopata, E., "Measurements of Electron-Temperature in A Capacitively Coupled Plasma Using Emission-Spectroscopy," *Journal of Vacuum Science & Technology A-Vacuum Surfaces and Films*, vol. 6, no. 3, pp. 2051-2053, 1988.
- [12] Norlén, G., "Wavelengths and Energy Levels of ArI and ArII based on New Interferometric Measurements in the Region 3400-9800 A," *Physica Scripta*, vol. 8 pp. 249-268, 1973.
- [13] B. Chapman, *Glow discharge processes*, p. 119, Wiley, New York (1980).
- [14] B. Chapman, *Glow discharge processes*, p. 118, Wiley, New York (1980).
- [15] A. J. van Roosmalen, J. A. G. Baggerman and S. J. H. Brader, *Dry Etching for VLSI*, p. 92, Plenum Press, New York and London (1991).